FOURTEENTH EUROPEAN ROTORCRAFT FORUM

Paper No. 71

ANALYTICAL STUDY OF DYNAMIC RESPONSE OF HELICOPTER IN AUTOROTATIVE FLIGHT

Yoshinori Okuno and Keiji Kawachi

Research Center for Advanced Science and Technology
University of Tokyo
4-6-1, Komaba, Meguro-ku, Tokyo, 146 JAPAN

Akira Azuma

Metropolitan Institute of Science and Technology

and

Shigeru Saito

National Aerospace Laboratory

20-23 September, 1988

MILANO, ITALY

ASSOCIAZIONE INDUSTRIE AEROSPAZIALI
ASSOCIAZIONE ITALIANA DI AERONAUTICA ED ASTRONAUTICA

Analytical Study of Dynamic Response of Helicopter in Autorotative Flight

Yoshinori Okuno and Keiji Kawachi
University of Tokyo

Akira Azuma
Metropolitan Institute of Science and Technology

and

Shigeru Saito
National Aerospace Laboratory

A nonlinear optimal control problem minimizing the touchdown speed of a helicopter in the autorotative flight following power failure is studied. The motion of the helicopter is expressed by the longitudinal three degree-of-freedom equations, and the rotor aerodynamic performance is calculated by using blade element theory combined with empirically modified momentum theory. This modified model has the ability of estimating the rotor thrust, H-force and torque properly even in vortex-ring state, including the effects of blade stall. This optimal control problem is, then, solved by using a numerical solution technique called *SCGRA*[1]. Results indicate that pilots should postpone the collective pitch flare. The effects of the time delay in the collective pitch reduction and/or of the climbing rate at the moment of power failure on the minimum touchdown speed are also presented. In addition, height-velocity diagrams for various gross weights and density altitudes are calculated by using the other numerical solution technique, dynamic programming. Results show good agreement with flight test data.

Notation

a = lift-curve-slope of blade element
B = tip loss factor
C_{d_0} = profile drag coefficient of blade element
C_{d_s} = drag coefficient of blade element in stall region
D = drag
h = height from ground, or distance above CG, see Fig.7
h_d = density altitude
J = nondimensional ground contact velocity, defined by Eq.(15)
L = lift
ℓ = distance behind CG, see Fig.7
m = mass of helicopter
n = load factor
P_a = available engine power
q = pitch rate, positive nose up
R = rotor radius
S = rotor disk area, or reference area
t = time from power failure
u = horizontal velocity
$\boldsymbol{u}$ = control vector
u_s = limitation of forward speed at touchdown
v = induced flow (nondimensionalized by $R\Omega$)
$\bar{v}$ = reference velocity defined by Eq.(2)
W = weight of helicopter
w = vertical velocity, positive descending
w_s = limitation of sinking rate at touchdown
$\boldsymbol{x}$ = state vector
x_s = radius of blade stall region, defined by Eq.(8.1) or Eq.(8.2)
α_R = angle of attack of rotor disk, defined by Eq.(3)
α_r = angle of attack of blade element at $0.75R$, defined by Eq.(17.4)
α_s = stalling angle of blade element
β_c = longitudinal flapping angle, positive nose down
γ = flight path angle, positive climbing, or Lock number
Θ = pitch attitude, positive nose up
θ_s = longitudinal cyclic pitch, positive nose up
θ_t = blade twist angle, positive twist up
θ_0 = collective pitch at $0.75R$
λ = inflow ratio, defined by Eq.(11.3)
μ = advance ratio, defined by Eq.(11.1)
ν = rate of descent, defined by Eq.(11.2)
σ = rotor solidity
Ω = rotor rotational speed

Subscripts

F = fuselage
f = time of touchdown
H = horizontal stabilizer
R = rotor
0 = time of power failure

Introduction

In case of power failure, a helicopter can safely land using autorotation. The control sequence during this autorotative flight is generally composed of the following five stages as shown in Fig.1:

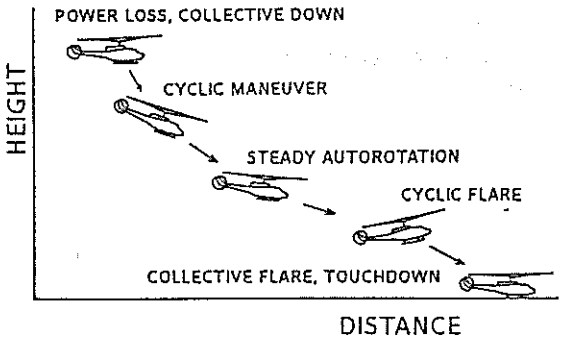

Fig. 1 Autorotative landing following power failure.

1) Reduction of the collective pitch just after power failure.
2) Control of the forward speed to achieve the minimum sinking rate.
3) Steady autorotative flight towards a landing point.
4) Nose up of the body to reduce the sinking rate and the forward speed.
5) Collective flare, that is, the rapid increase of the collective pitch in order to convert the rotating energy of the rotor blade into the thrust.

The delicate timing and the appropriate amplitude of the control are required throughout the entire flight stages. Especially, the stages 4) and 5) are important to land in safety, and the miscontrol in these stages causes the hard landing. The flight test is usually used in order to verify the safety of landing from the specified initial conditions. It, however, requires the expensive cost and risk.

In this paper, the analytical method using an optimal control theory based on variational method is developed in order to make clear the most safe sequence of control and/or flight path during the autorotative flight following power failure. These optimal informations are useful to reduce the cost and risk of the flight test. The application of the optimal control theory to the autorotative flight was first proposed by Komoda[2], and the recent numerical method was tried by Lee[3]. These analyses assume the simple point-mass model of the helicopter as well as the simple aerodynamic model, which reduces the accuracy of the solution and it's effectiveness. In this paper, a more realistic model is used to improve the accuracy of the solution, owing to the advancement of the computer and the numerical solution technique.

In addition to the study of the most safe control and flight path, the height-velocity diagrams (H-V diagrams) are also analyzed. The single engine helicopter has the avoidance flight region as schematically shown in Fig.2, which is usually obtained by the flight test. The empirical equations concerning the safety boundaries were proposed by Pegg[8], but it neglected the fundamental parameters, such as, the speed limit of the landing gears and/or the own characteristics of the helicopter motion. In this study, dynamic programming is applied to predict the H-V diagrams, because this method makes it possible to investigate the minimum touchdown speed for the various initial conditions without calculating each optimal path.

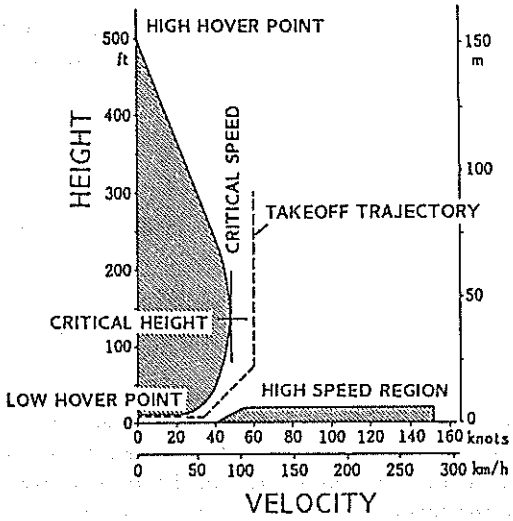

Fig. 2 Typical height-velocity diagram.

Rotor Performance in Autorotation

In the intermediate descending range between normal working state and windmill state, the induced flow is directed against the uniform flow and does not extend infinitely. Therefore, momentum theory cannot be applied theoretically to analyze the rotor performance in the autorotative flight following power failure. However, as far as the rotor angle of attack is not so large, momentum theory works well even in so-called vortex-ring state, empirically[4]. In this paper, a modified model of the induced flow is developed as follows:

Simple momentum theory is expressed as

$$\frac{\nu}{\bar{v}} = \left(\frac{v}{\bar{v}}\right)\sin^2\alpha_R \pm \sin\alpha_R\sqrt{\left(\frac{\bar{v}}{v}\right)^2 - \left(\frac{v}{\bar{v}}\right)^2\cos^2\alpha_R} \quad (1)$$

where

$$\bar{v} = \sqrt{C_T/2} \quad (2)$$

$$\alpha_R = \tan^{-1}(\nu/\mu) \quad (3)$$

The solution of Eq.(1) is indicated in Fig.3 by dotted lines. It is observed that this solution is discontinuous and smaller than the experimental results[4] in vortex-ring state. In order to overcome these defects, Eq.(1) is modified introducing two coefficients C_1, C_2 as follows:

$$\frac{\nu}{\bar{v}} = \left(\frac{v}{\bar{v}}\right)^{C_1}\sin^2\alpha_R \pm \sin\alpha_R \cdot\sqrt{\left(\frac{\bar{v}}{v}\right)^2 - \left(\frac{v}{\bar{v}}\right)^2\left(C_2\sin^2\alpha_R + \cos^2\alpha_R\right)} \quad (4)$$

where

$$C_1 = \frac{1}{2} \quad (5.1)$$

$$C_2 = \left(1+\sqrt{2}\right)^{-4} \quad (5.2)$$

The solution of Eq.(4) is also indicated in Fig.3 by a solid line. It is observed that this modified model can give more realistic induced flow over the entire range of the flight conditions. The effect of the modification becomes negligible small and Eq.(4) nearly equals to Eq.(1) when the rotor angle of attack is not so large.

Referring to Wolkovitch[6], the vortex-ring state occurs when the relative velocity of the vortex cores normal to the disk falls to zero, that is,

$$-\nu + v/2 = 0 \tag{6}$$

Fig.4 shows the result of Eq.(6) combined with Eq.(4). The broken lines indicate the boundaries of the region where the fluctuations of the thrust were observed in the experiments[4]. It is observed that Eq.(6) gives the condition for the most severe vortex-ring state, but the fluctuations of the thrust decrease as the rotor angle of attack decreases.

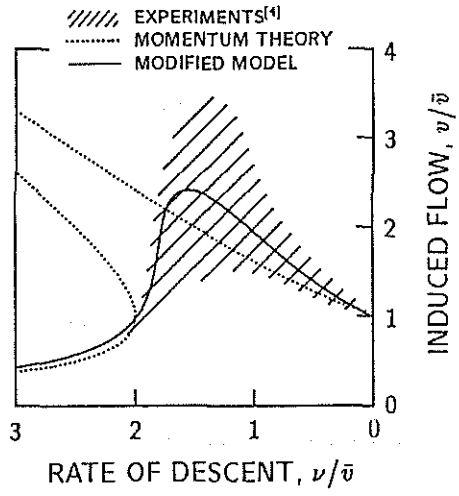

Fig. 3 Induced flow in vertical flight.

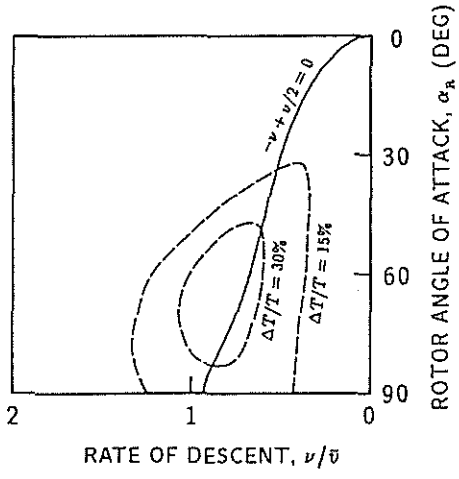

Fig. 4 Boundary of vortex-ring state.

Thrust, H-force, and torque coefficients are described by using blade element theory as

$$C_T = \frac{1}{2}a\sigma\Big\{\frac{(B^3 - x_s{}^3)}{3}\theta_0 - \frac{(B^2 - x_s{}^2)}{2}\lambda + \frac{(B^2 - x_s{}^2)}{2}\mu\theta_s\Big\} \tag{7.1}$$

$$C_H = \frac{1}{4}\sigma\{(1 - x_s{}^4)C_{d_0} + x_s^4 C_{d_s}\}\mu + \frac{1}{2}a\sigma\Big[\{\frac{(B^2 - x_s{}^2)}{4}\theta_s + \frac{(B - x_s)}{2}\mu\theta_0\}\lambda + \{-\frac{(B^3 - x_s{}^3)}{3}\theta_0 + \frac{3(B^2 - x_s{}^2)}{4}\lambda - \frac{(B^2 - x_s{}^2)}{4}\mu\theta_s + \frac{(B^2 - x_s{}^2)}{4}\mu\beta_c\}\beta_c\Big] \tag{7.2}$$

$$C_Q = \frac{1}{8}\sigma\{(1 - x_s{}^4)C_{d_0} + x_s^4 C_{d_s}\} + \frac{1}{2}a\sigma\Big[\{\frac{(B^3 - x_s{}^3)}{3}\theta_0 - \frac{(B^2 - x_s{}^2)}{2}\lambda + \frac{(B^2 - x_s{}^2)}{4}\mu\theta_s\}\lambda + \{-\frac{(B^4 - x_s{}^4)}{8}\theta_s - \frac{(B^2 - x_s{}^2)}{2}\mu\lambda - \frac{(B^4 - x_s{}^4)}{8}\beta_c\}\beta_c\Big] \tag{7.3}$$

where x_s is the radius of blade stall, which is given by

for the simple model,

$$x_s = 0 \tag{8.1}$$

for the modified model,

$$x_s = \frac{1}{-2\theta_t}\Big[\sqrt{\Big\{\alpha_s - \big(\theta_0 - \frac{3}{4}\theta_t\big)\Big\}^2 + 4\theta_t\lambda} - \Big\{\alpha_s - \big(\theta_0 - \frac{3}{4}\theta_t\big)\Big\}\Big] \tag{8.2}$$

The solutions of the present modified model and the simple momentum model are calculated by using Eq.(1) & Eq.(8.1), and Eq.(4) & Eq.(8.2), respectively. Fig.5 and Fig.6 show the collective pitch angles and the torque coefficients required to generate the constant thrust, $C_T/\sigma = 0.08$ calculated by using these two models, which are compared with experimental data[5]. The result by using the present modified model shows the better agreement with the experimental data over the entire range of the flight condition, from hovering to windmill state.

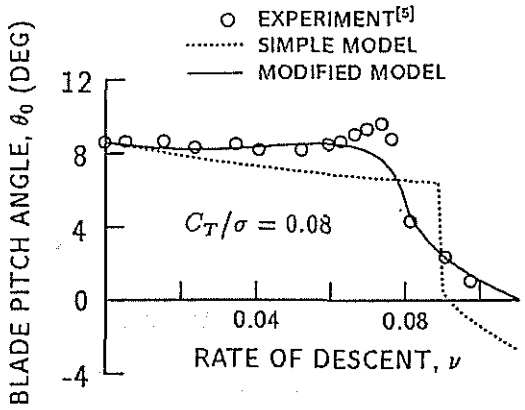

Fig. 5 Blade pitch angles for constant thrust in vertical descent.

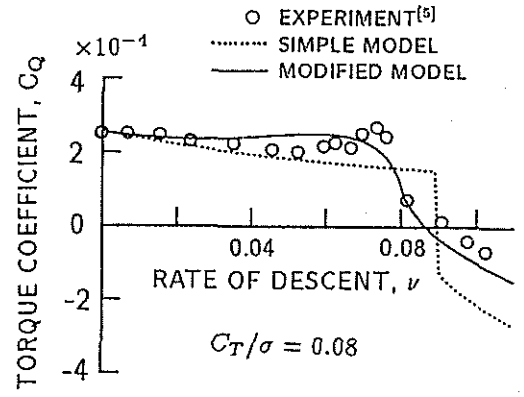

Fig. 6 Necessary torque for constant thrust in vertical descent.

Dynamic Model of a Helicopter

The motion of the helicopter is considered to be limited in the longitudinal plane as shown in Fig.7. The equations of motion are described as follows:

$$\frac{dh}{dt} = w \tag{9.1}$$

$$\frac{du}{dt} = -\frac{1}{m}(T\sin\Theta + H\cos\Theta + D_F\cos\alpha_F) \tag{9.2}$$

$$\frac{dw}{dt} = -\frac{1}{m}(T\cos\Theta - H\sin\Theta + D_F\sin\alpha_F) + g \tag{9.3}$$

$$\frac{d\Omega}{dt} = -\frac{1}{I_R}\cdot\left(Q - \frac{P_s}{\Omega}\right) \tag{9.4}$$

$$\frac{d\Theta}{dt} = q \tag{9.5}$$

$$\frac{dq}{dt} = -\frac{1}{I_{By}}(-T\cdot\ell_R + H\cdot h_R - L_H\cdot\ell_H) \tag{9.6}$$

where

$$T = C_T\rho SR^2\Omega^2 \tag{10.1}$$
$$H = C_H\rho SR^2\Omega^2 \tag{10.2}$$
$$Q = C_Q\rho SR^3\Omega^2 \tag{10.3}$$

The coefficients C_T, C_H, and C_Q are given by Eqs.(7.1-3). The advance ratio μ, the descending rate ν, and the inflow ratio λ are given by

$$\mu = \Big\{(u - h_R\cdot q)\cos(\Theta - \beta_c) - (w + \ell_R\cdot q)\sin(\Theta - \beta_c)\Big\}/R\Omega \tag{11.1}$$

$$\nu = \Big\{(u - h_R\cdot q)\sin(\Theta - \beta_c) + (w + \ell_R\cdot q)\cos(\Theta - \beta_c)\Big\}/R\Omega \tag{11.2}$$

$$\lambda = -\nu + v \tag{11.3}$$

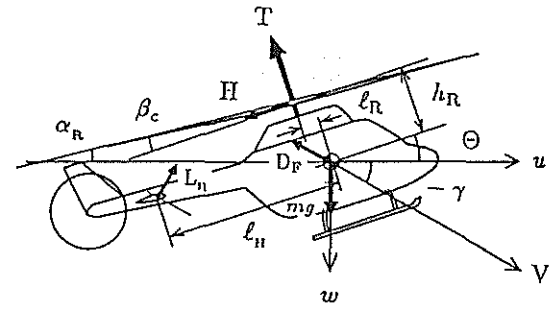

Fig. 7 Helicopter model.

The longitudinal flapping angle β_c is given by

$$\beta_c = -\theta_s - \left(\frac{8}{3}\theta_0 - 2\lambda\right)\mu + \frac{16}{\gamma}\cdot\frac{q}{\Omega} \tag{12}$$

The lift of the horizontal stabilizer L_H is given by

$$L_H = \frac{1}{2}\rho(u^2 + w^2)S_H C_{L_H} \tag{13.1}$$

$$C_{L_H} = a_{H_0}\cdot\frac{1}{2}\sin 2\alpha_H \tag{13.2}$$

$$\alpha_H = \Theta + \tan^{-1}\{(w + \ell_H\cdot q)/u\} \tag{13.3}$$

where a_{H_0} is the lift-curve-slope of the horizontal stabilizer at $\alpha_H = 0$.

Finally, the horizontal and vertical components of the drag of the body are given by

$$\alpha_F = \tan^{-1}(w/u) \tag{14.1}$$

$$D_F\cos\alpha_F \simeq \frac{1}{2}\rho u^2 S_F C_{D_F} \tag{14.2}$$

$$D_F\sin\alpha_F \simeq 0 \tag{14.3}$$

These state equations cannot be explicitly solved because $C_T, v, \mu, \nu, \lambda, \beta_c$ are dependent each other. Therefore, the iterative calculations are required at each time step.

Formulation of Optimal Landing Problem

The primary objective of the autorotative flight following power failure is to land in safety with allowable touchdown speed. Therefore, the maneuver in autorotative flight is analyzed by using optimal control theory to solve the problem of minimizing the touchdown speed. The maximum value of the allowable touchdown speed depends on the landing gear design. In the case of wheel-type landing gear, horizontal component of the ground contact velocity is allowed to be fairly large.

In this study, the performance function is defined as

$$J = \sqrt{\left(\frac{u(t_f)}{u_s}\right)^2 + \left(\frac{w(t_f)}{w_s}\right)^2} \quad \rightarrow min. \qquad (15)$$

and the boundary conditions are given by

$$h(0),\ u(0),\ w(0),\ \Omega(0),\ \Theta(0),\ q(0)\ ;given \qquad (16.1)$$
$$h(t_f),\ \Theta(t_f)=0,\ q(t_f)=0 \quad ;specified \qquad (16.2)$$

The range of the collective pitch angle and the cyclic pitch angle are mechanically limited, and the range of the pitch attitude is limited by the handling quality. In addition, two more limits are imposed, the one is the limit on the angle of attack of the blade element at $0.75R$, and the other is the limit on the load factor. These five limits are formulated as inequality constraints as follows:

$$\theta_{0min} \leq \theta_0 \leq \theta_{0max} \qquad (17.1)$$

$$\theta_{smin} \leq \theta_s \leq \theta_{smax} \qquad (17.2)$$

$$\Theta_{min} \leq \Theta \leq \Theta_{max} \qquad (17.3)$$

$$\alpha_r = \theta_0 - \frac{4}{3}\lambda \leq \alpha_{max} \qquad (17.4)$$

$$\frac{dw}{dt} \geq g\,(1 - n_{max}) \qquad (17.5)$$

For the usage of variational method, these inequality constraints are transformed into equality constraints by introducing five additional control variables and two additional state variables called "slack variables"[9] as follows:

$$\theta_0 = \theta_{0_r} \sin\theta_{0d} + \theta_{0_a} \qquad (18.1)$$

$$\theta_s = \theta_{s_r} \sin\theta_{sd} + \theta_{s_a} \qquad (18.2)$$

$$\frac{dq}{dt} = \Theta_r(-\dot{\Theta}_d^2 \sin\Theta_d + \ddot{\Theta}_d \cos\Theta_d) \qquad (18.3)$$

$$\theta_0 - \frac{4}{3}\lambda = \alpha_{max} - \frac{1}{2}{\alpha_d}^2 \qquad (18.4)$$

$$\frac{dw}{dt} = g\left\{(1 - n_{max}) + \frac{1}{2}{n_d}^2\right\} \qquad (18.5)$$

In all, the dimension of the state vector becomes 8, and the dimension of the control vector becomes 7. They are given by

$$x = (h, u, w, \Omega, \Theta, q, \Theta_d, \dot{\Theta}_d)^T \qquad (19.1)$$
$$u = (\theta_0, \theta_s, \theta_{0d}, \theta_{sd}, \ddot{\Theta}_d, \alpha_d, n_d)^T \qquad (19.2)$$

and, the following two differential equations for the new state variables are added to the state equations Eqs.(9.1-6):

$$\frac{d\Theta_d}{dt} = \dot{\Theta}_d \qquad (20.1)$$
$$\frac{d\dot{\Theta}_d}{dt} = \ddot{\Theta}_d \qquad (20.2)$$

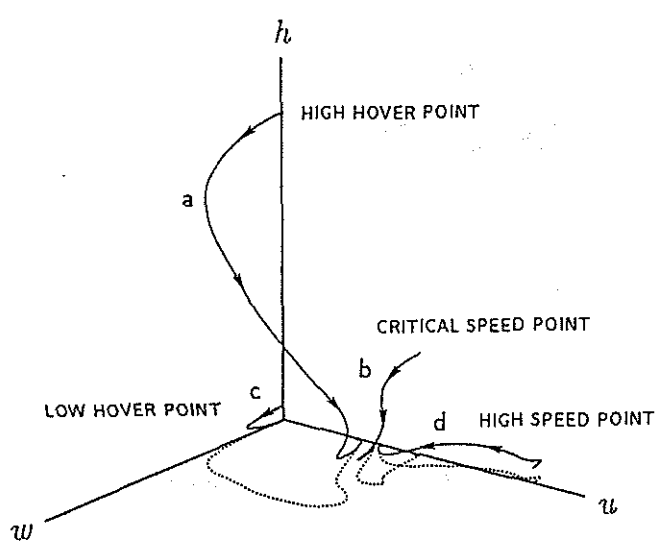

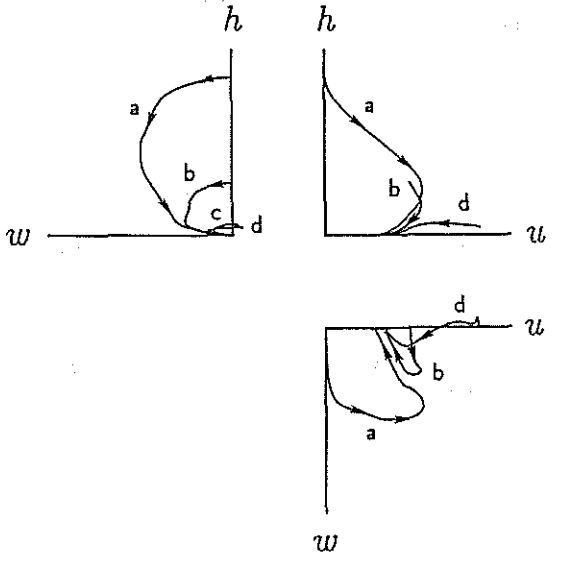

Fig. 8 Optimal landing trajectories.

Theoretical Results in Comparison with Flight Test Data

The flight paths to minimize the touchdown speed are analyzed for an exemplified helicopter, the specifications of which are presented in Table 1, with the four initial conditions shown in Fig.8. This nonlinear optimal control problem with equality constraints is solved by using a numerical solution technique called *SCGRA*[1]. The optimal control sequences for these four initial conditions are discussed as follows:

Landing from High Hover Point

Fig.9 shows the optimal solution and the flight test data[7] for landing from high hover point. Theoretical results are in good agreement with the flight test data in the pitching motion but not in the collective pitch input. Fig.10 compares the optimal path with the predicted flight test path which is calculated by using the time history of the collective pitch input of the flight test data. The premature collective flare results in the hard ground contact because of the loss of the rotor rotational energy.

Fig.11 shows the time history of the load factor and the blade angle of attack during the optimal landing from a high hover point. It is observed that the blade pitch during the collective flare is limited by the load factor for the earlier period and limited by the blade angle of attack for the later period.

Helicopters cannot avoid to encounter the vortex-ring state if the power fails in hover. Fig.12 shows the locus of optimal landing path in $\alpha_R - \nu/\bar{v}$ plane. Numerals in the figure denote the time elapsed from the power failure in second. In this case, the helicopter is in the vortex-ring state for the first two seconds. During this period, the collective pitch is reduced to the minimum value and the cyclic pitch holds the constant value as shown in Fig.9. Therefore, it is assumed that the vortex-ring does not cause the loss of control.

Table 1. Specifications of the exemplified helicopter.

maximum gross weight,	W	=	5900 (kg)
rotor radius,	R	=	8.534 (m)
blade chord,	c	=	0.381 (m)
number of blades,	b	=	4
rotor rotational speed,	Ω	=	25.03 (rad/s)
rotor moment of inertia,	I_R	=	7107 (kgm^2)
location of CG,	ℓ_R	=	0.0254 (m)

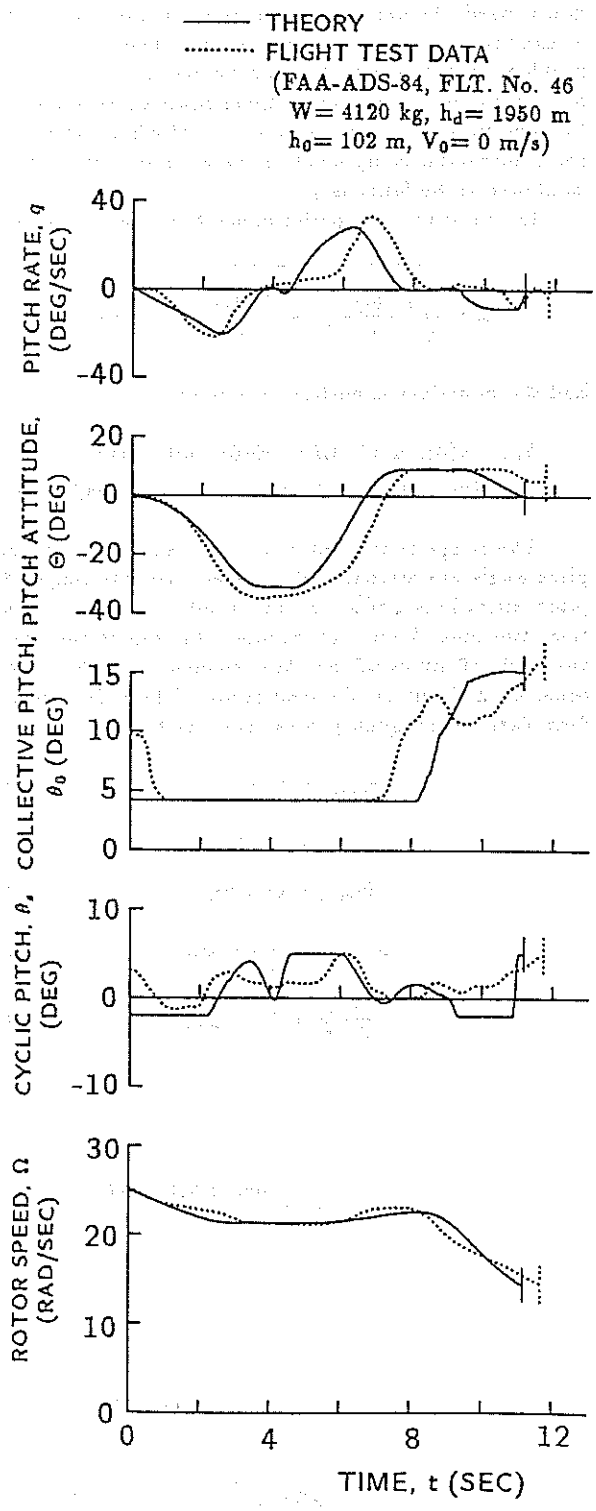

Fig. 9 Comparison of optimal solution with flight test landing from high hover point.

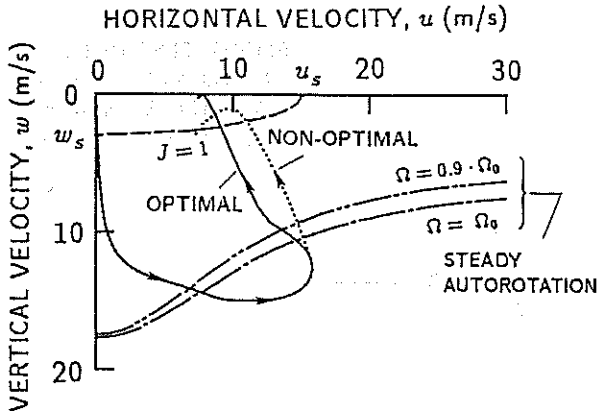

Fig. 10 Comparison between optimal and non-optimal landing trajectories from a high hover point.

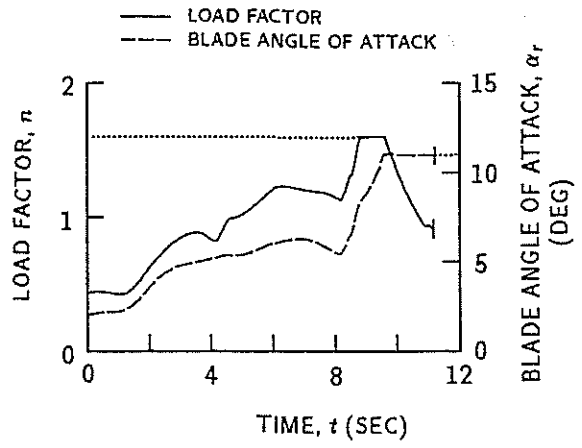

Fig. 11 Time history of optimal landing from high hover point.

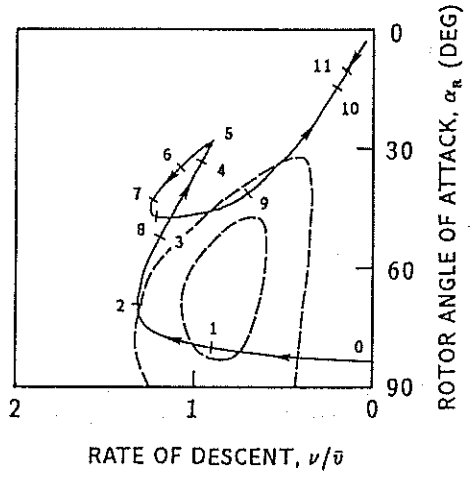

Fig. 12 Locus of optimal landing trajectory from high hover point.

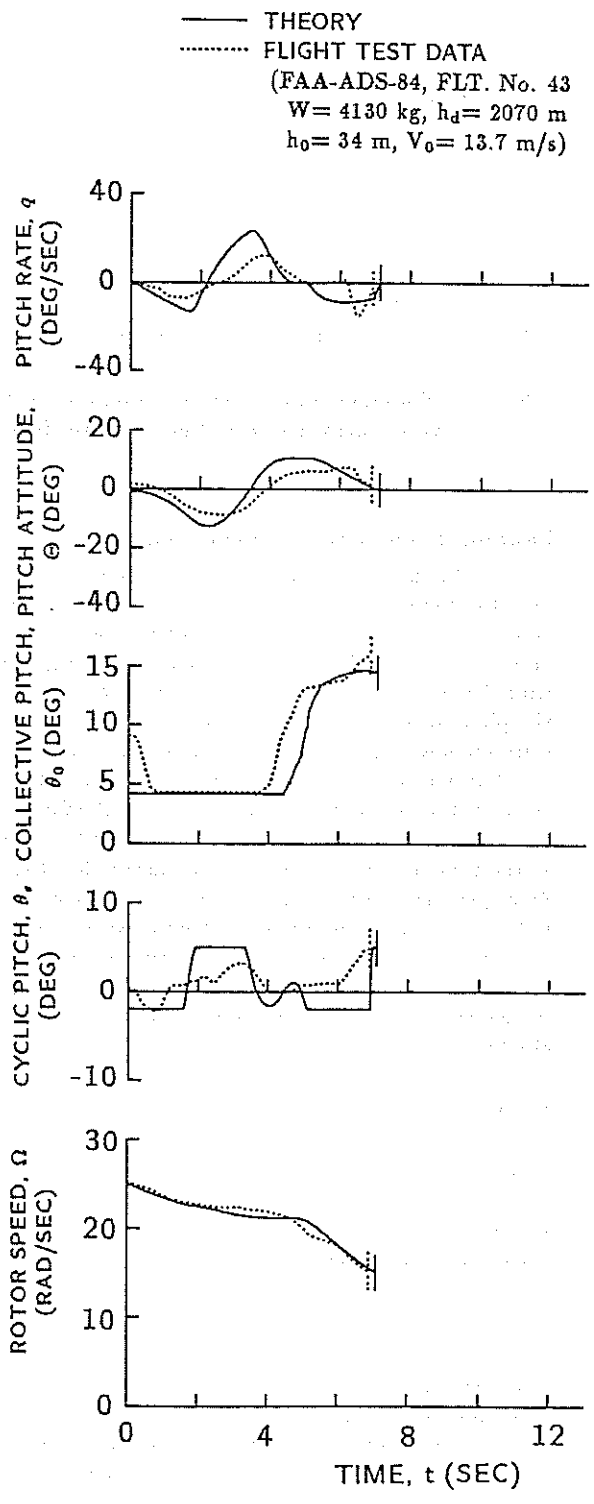

Fig. 13 Comparison of optimal solution with flight test landing from critical speed point.

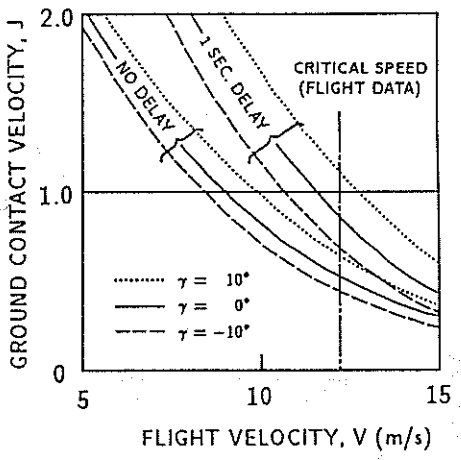

Fig. 14 Minimum landing velocity from critical height versus flight speed at time of power failure.

Landing from Critical Speed Point

Fig.13 shows the result for critical speed point. In this case the flight time from the power failure to the touchdown is much shorter than that of the landing from the high hover point. Therefore, the influence of neglecting the time delay in the control inputs are not small especially in the pitching motion. It follows that the theoretical results estimate lower critical speed than the flight test data.

Estimation of critical speed point is important for decision of the takeoff trajectory. However, the flight tests for H-V diagrams are conducted generally with the level flights at the time of power failure. Fig.14 shows the effects of the flight path angle and the time delay in initial collective pitch reduction on the minimum touch down speed. The ground contact velocity increases with the climbing rate at the time of power failure and also the influence of one second delay in the collective pitch reduction is more remarkable as the climbing rate increases.

Landing from Low Hover Point

Fig.15 shows the results for low hover point. The test pilot didn't reduce the collective pitch following power failure in contrast to the optimal solution. This difference is caused by neglecting the time delay in the collective pitch operation in the present analysis.

Landing from High Speed Region

Fig.16 shows only theoretical result for high speed region. Experimental data are not available for this region. In this case, the cyclic pitch is controlled to nose-up throughout the time from the power loss to the touchdown because not only the sinking rate but also the forward speed is critical for the safe landing.

In high speed region, the initial kinetic energy of helicopter is enough for the safe landing, therefore estimation of the longitudinal maneuverability including pilot's reaction time is significant for estimation of the avoidance region.

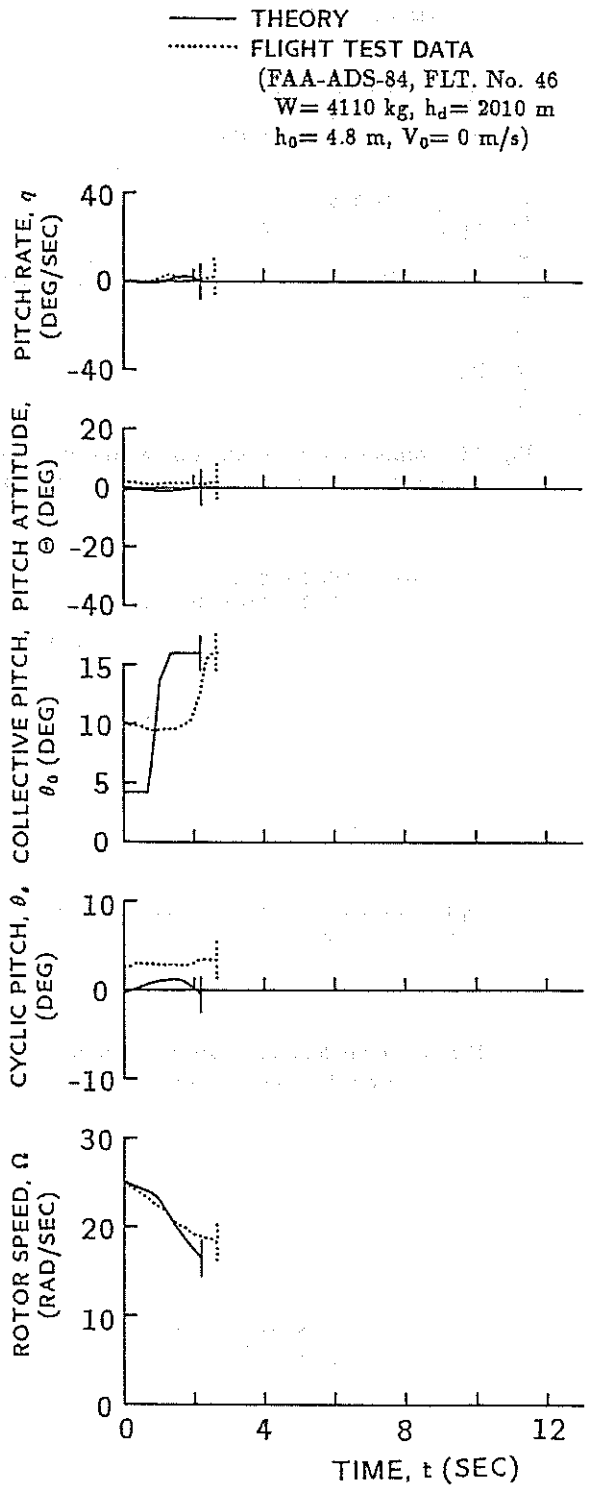

Fig. 15 Comparison of optimal solution with flight test landing from low hover point.

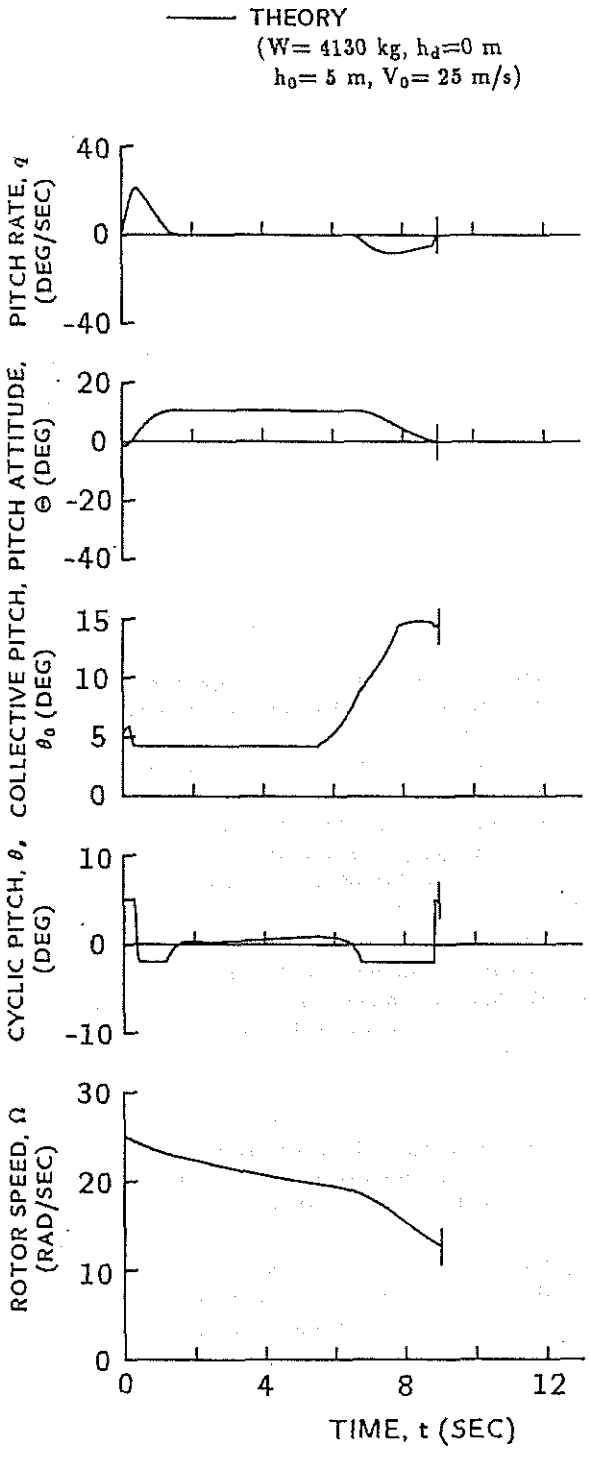

Fig. 16 Time history of optimal landing from high speed region.

Analytical Prediction of H-V Diagram Using Dynamic Programming

Height-velocity diagram can be obtained as a contour line in H-V plane on which the minimum ground contact velocity J equals 1. The optimal control theory based on variational method gives the good results as mentioned in the previous section when calculating a particular optimal path. However, this method requires many cases of calculation with the various initial heights and velocities to obtain the entire H-V diagrams. Here, the other optimal control theory called dynamic programming is used to estimate the H-V diagrams. Although this method costs more computation time (several times in this study) than variational method when calculating particular optimal paths, dynamic programming makes it possible to calculate the minimum touchdown speed for the various entry conditions without calculating each optimal path. Therefore, dynamic programming is selected in order to estimate the H-V diagrams in this study.

Although recent development in the super computers extends the applicability of dynamic programming, it is still required in this study to simplify the equations of motion of the helicopter. The inertia of the pitching motion is neglected and the helicopter is assumed to be a point-mass. Dynamic programming has the merit to formulate inequality constraints on the control variables and/or on the state variables without transformation into equality constraints. This makes it possible to avoid the increase of the dimension of the control vector. As a result, the state variables and the control variables are

$$x = (u, w, \Omega)^T \tag{21.1}$$

$$u = (\theta_0, \Theta)^T \tag{21.2}$$

Height h is selected to the independent variable because it is necessary for dynamic programming that the terminal time is fixed and the state variables are not specified at the terminal time.

Fig.17 shows the H-V diagrams of the exemplified helicopter with three combinations of gross weights and density altitudes. The solid lines indicate the results with the present modified model and the broken lines indicate the results with simple momentum model. It is observed that the present modified model shows the better agreement with the flight test data. Theoretical results estimate the avoidance region smaller than the flight test data because the time delay in the pitching motion is neglected in this study. In addition, the possibility of the non-optimal control is included in the flight test.

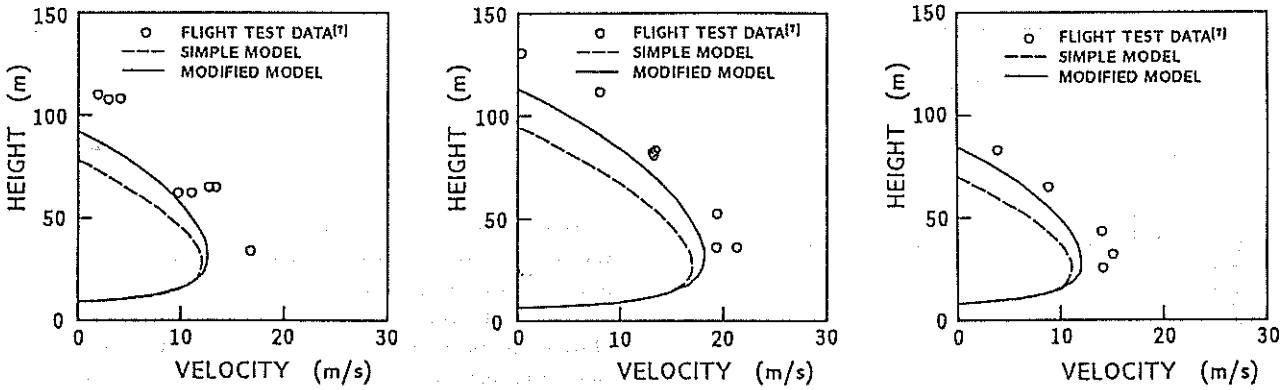

(1) W = 4130 kg, h_d = 1620 m (2) W = 4580 kg, h_d = 1510 m (3) W = 4580 kg, h_d = -210 m

Fig. 17 Comparison of height-velocity diagrams.

Conclusion

Nonlinear optimal control theory based on variational method is well applied to analyze the minimum touchdown speed in autorotative flight of a helicopter following power failure. In addition, dynamic programming is applied to predict height-velocity diagrams. It is indicated that these applications of the optimal control theory have the possibility to improve the maneuver procedure shown by the flight tests and to extend the safety boundary empirically determined.

The following results are also drawn:

1) Pilots tend to conduct collective flare earlier than the theoretical optimal timing.
2) Critical speed increases with climbing rate at the moment of power failure.
3) The modified model of the rotor performance can give the more realistic prediction of the height-velocity diagrams.

References

[1] Wu, A. K., and Miele, A.: "Sequential Conjugate Gradient Restoration Algorithm for Optimal Control Problems with Non-Differential Constraints and General Boundary Conditions, Part 1," *Optimal Control Applications and Methods*, Vol.1, 1980.

[2] Komoda, M.: "An Analytical Method to Predict Height-Velocity Diagram and Critical Decision Point of Rotorcraft," NAL TR-245 (in Japanese), 1971.

[3] Lee, A. Y., Bryson, A. E., Jr., and Hindson W. S.: "Optimal Landing of a Helicopter in Autorotation," *Journal of Guidance and Control*, Vol.11, No.1, 1988.

[4] Washizu, K., Azuma, A., Koo, J., and Oka, T.: "Experiments on a Model Helicopter Rotor Operating in the Vortex-Ring State," *Journal of Aircraft*, Vol.3, No.3, 1966.

[5] Castles, W., Jr., and Gray, R. B.: "Empirical Relationship Between Induced Velocity, Thrust and Rate of Descent of a Helicopter Rotor as Determined by Wind Tunnel Tests on Four Model Rotors," NACA TN 2474, 1951

[6] Wolkovitch, J.: "Analytical Prediction of Vortex-Ring Boundaries for Helicopters in Steep Descents," *Journal of the American Helicopter Society*, Vol.17, No.3, 1972.

[7] Hanley, W. J., DeVore, G., and Martin, S.: "An Evaluation of the Height Velocity Diagram of a Heavy Weight, High Rotor Inertia, Single Engine Helicopter," FAA-ADS-84, 1966.

[8] Pegg, R. J.: "An Investigation of the Helicopter Height-Velocity Diagram Showing Effects of Density Altitude and Gross Weight," NASA TN D-4536, 1968

[9] Jacobson, D. H., and Lele, M. M.: "A Transformation Technique for Optimal Control Problems with a State Variable Inequality Constraint," *IEEE Transactions on Automatic Control*, Vol.AC-14, No.5, 1969.